AIAA JOURNAL
Vol. 40, No. 9, September 2002

Control Stability Analysis of Smart Beams with Debonded Piezoelectric Actuator Layer

Dongchang Sun* and Liyong Tong†
University of Sydney, Sydney, New South Wales 2006, Australia

Debonding of a piezoelectric actuator or sensor layer in an actively controlled structure may significantly affect its closed-loop control and even collapse the active control. Investigation of the effects of the debonded piezoelectric layer on the control stability of smart structures is very important. A state-equation-based method is presented to investigate the control stability of the beams controlled by partially debonded piezoelectric actuator and sensor layers. An analytical model of a beam with a debonded piezoelectric layer is given, in which the debonding of the piezoelectric layer is modeled by considering the adhesive layers. Both displacement continuity and force equilibrium conditions are imposed at the interfaces between the debonded and perfectly bonded regions. Based on this model, a characteristic equation for the controlled structure with debonded piezoelectric actuators and sensor is derived, from which the eigenvalues of the controlled system can be obtained. The control stability of a controlled mode can be evaluated by examining the sign of the real part of the corresponding eigenvalue. The simulation results show that even a 5% edge debonding of the actuator layer can destabilize the cantilevered beam controlled by an actuator/sensor pair, whereas a beam controlled by a self-sensing actuator layer can tolerate much larger edge debonding of the piezoelectric layer. More significant changes can be found in both the damping coefficient and the frequency of the mode whose frequency is close to one of the modal frequencies of the debonded part of the actuator.

Nomenclature

a	=	coordinate of interface between bonded and debonded regions
b	=	width of the composite beam
E	=	Young's modulus
e_{31}	=	piezoelectric stress constant
f_l	=	axial loads per unit length
f_t	=	transverse loads per unit length
g	=	control gain
I	=	current output of sensor
M	=	bending moment
Q	=	shear stress resultant
q	=	charge output of sensor
T	=	normal stress resultant
u	=	longitudinal displacement
V	=	control voltage
w	=	transverse displacement
λ	=	eigenvalue
ν	=	Poisson's ratio
ρ	=	equivalent mass density

Subscripts and Superscripts

$v1$	=	upper bonding layer
$v2$	=	lower bonding layer
1	=	actuator layer
2	=	host beam
3	=	sensor layer

I. Introduction

VIBRATION control of flexible structures using distributed piezoelectric sensors and actuators has been extensively studied in the past decade.[1–7] The new piezoelectric materials are capable of generating larger strain under a higher electric field. For example, the piezoelectric single crystals can generate a high strain up to 1.4% and can sustain very high electric fields up to the order of 10 MV/m without electric breakdown. Consequently, the possibility of debonding of the piezoelectric actuator from the host greatly increases, particularly in dynamic circumstances. When debonding between the piezoelectric actuator/sensor layers and the host structures occurs, it will result in significant changes of the structures, particularly for closed-loop case, and may even destabilize the closed-loop control. Thus, it is of great significance to investigate the effects of the actuator debonding on dynamic and closed-loop control of smart structures.

Recently, increasing attention has been paid to the dynamic effects caused by imperfect bonding of piezoelectric transducers on open-loop and closed-loop systems. Seeley and Chattopadhyay[8,9] developed refined higher-order finite element models (FEM) of beams and plates with debonded piezoelectric layers/patches and investigated the effects of the debonding of the piezoelectric actuators on dynamic properties of the open- and closed-loop systems by numerical analysis and experiment. Wang and Meguid[10] examined the effect of interfacial debonding of the actuator patch on stress distribution based on singular integral equations. Tylikowski[11] presented a bending–extensional model of a beam with edge debonded piezoelectric patches. Tong et al.[12] developed another bending–extensional model by considering both peel and shear stresses in the adhesive layers and investigated the sensing and actuating behaviors of the debonded sensor/actuator. Rew et al.[13] provided a real-time frequency estimation method to guarantee robust vibration control of a delaminated beam by using a positive feedback controller.

Most of the research focuses on the effects of the actuator debonding on the dynamic behavior of the smart structures for open-loop and closed-loop cases. However, it may be of more concern if a closed-loop system is still usable after the occurrence of an actuator debonding without adjusting the original setup. One method of judging the failure of a control system is to determine the stability of the important modes. If one mode, which was originally stable before the debonding occurs, becomes unstable after debonding, the original system will be completely destroyed by the debonding. Therefore, an effective scheme to determine the stability of the system with a debonded actuator/sensor is needed.

In this paper, a method of determining the control stability of a controlled beam with partially debonded piezoelectric actuator

Received 18 November 2001; revision received 5 April 2002; accepted for publication 10 April 2002.

*ARC Research Associate, School of Aerospace, Mechanical and Mechatronic Engineering.

†Associate Professor, School of Aerospace, Mechanical and Mechatronic Engineering. Senior Member AIAA.

and sensor is presented. First, an analytical model of a beam with debonded piezoelectric layer is established in which both transverse and longitudinal vibration of the host beam, the piezoelectric layers, and the adhesive layers are considered. The debonding of the piezoelectric layer is modeled by assuming that the adhesive layers in the debonding region does not transfer any peel and shear stresses between the host beam and the actuator layer. Both displacement continuity and force equilibrium conditions are imposed at the interfaces between the debonded and perfectly bonded regions. Then, based on this model, a characteristic equation for the controlled beam with debonded piezoelectric actuators and sensor is derived. The eigenvalues obtained from the characteristic equation can be used to determine if the controlled modes are stable after a debonding of the actuator occurs. Finally, simulation examples are given to evaluate the effect of an edge debonding of the actuator layer on the control stability of a cantilevered beam controlled by a proportional and derivative (PD) controller.

II. Mathematical Model of Beam with Debonded Actuator/Sensor Layer

Consider a slender composite beam with length L, on which two piezoelectric layers are bonded onto its upper and lower surfaces as actuator and sensor, respectively, as shown in Fig. 1. An edge debonding between the piezoelectric layer and the host beam is introduced at the right end of the beam. It is assumed that the debonding occurs throughout the width of the beam and the debonding front lines are straight and perpendicular to the x axis. The adhesive layers are assumed to carry constant transverse shear and peel strains due to their thinness. In the debonded region, it is assumed that there is no stress transferring between the host beam and piezoelectric actuator or sensor layer. In addition, contact and friction between the two debonded surfaces are not considered for simplicity.

The equations of motion of the composite beam can be derived as[14]

$$\rho_1 b h_1 u_{1,tt} = T_{1,x} + b\tau_1 \tag{1a}$$

$$\rho_1 b h_1 w_{1,tt} = Q_{1,x} + b\sigma_1 \tag{1b}$$

$$M_{1,x} + b\tau_1 h_1/2 - Q_1 = 0 \tag{1c}$$

$$\rho_2 b h_2 u_{2,tt} = T_{2,x} - b\tau_1 + b\tau_3 + f_l(x,t) \tag{2a}$$

$$\rho_2 b h_2 w_{2,tt} = Q_{2,x} - b\sigma_1 + b\sigma_3 + f_t(x,t) \tag{2b}$$

$$M_{2,x} + b(\tau_1 + \tau_3)h_b/2 - Q_2 = 0 \tag{2c}$$

$$\rho_3 b h_3 u_{3,tt} = T_{3,x} - b\tau_3 \tag{3a}$$

$$\rho_3 b h_3 w_{3,tt} = Q_{3,x} - b\sigma_3 \tag{3b}$$

$$M_{3,x} + b\tau_3 h_3/2 - Q_3 = 0 \tag{3c}$$

The axial stress resultants and bending moments for the actuator, the host beam, and the sensor can be written as follows:

$$T_1 = E_1 b h_1 u_{1,x} - b e_{311} V(t), \qquad M_1 = -\left(E_1 b h_1^3/12\right) w_{1,xx}$$

$$T_i = E_i b h_i u_{i,x}, \qquad M_i = -\left(E_i b h_i^3/12\right) w_{i,xx}, \qquad i = 2, 3 \tag{4}$$

When the constant shear and peel strain assumption is used, the shear and peel stress in the adhesive layer are given by

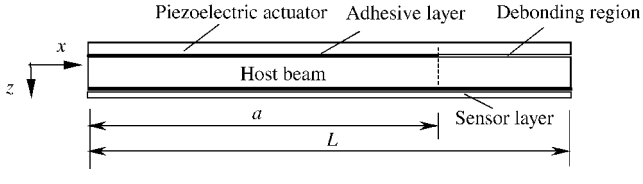

Fig. 1 Beam with partially debonded piezoelectric actuator/sensor layer.

$$\tau_1 = k_1 \frac{E_{v1}}{2(1+\nu_{v1})h_{v1}}\left[\frac{h_1}{2}w_{1,x} + \frac{h_2}{2}w_{2,x} + (u_2 - u_1)\right]$$

$$\sigma_1 = \frac{k_1 E_{v1}(1-\nu_{v1})}{(1-2\nu_{v1})(1+\nu_{v1})h_{v1}}(w_2 - w_1)$$

$$\tau_3 = k_3 \frac{E_{v3}}{2(1+\nu_{v3})h_{v3}}\left[\frac{h_2}{2}w_{2,x} + \frac{h_3}{2}w_{3,x} + (u_3 - u_2)\right]$$

$$\sigma_3 = \frac{k_3 E_{v3}(1-\nu_{v3})}{(1-2\nu_{v3})(1+\nu_{v3})h_{v3}}(w_3 - w_2) \tag{5}$$

where k is a parameter describing the bonding condition.

Debonding:

$$k_i = 0, \qquad i = 1, 3 \tag{6a}$$

Perfect bonding:

$$k_i = 1, \qquad i = 1, 3 \tag{6b}$$

Equation (6) indicates that the peel and shear stresses in the adhesive layer are zero in the debonded regions.

III. Sensor Equation and Control Law

The electric charge accumulated on the electrodes of the sensor layer due to the direct piezoelectric effect can be evaluated by

$$q(t) = \int_0^a b e_{313} u_{3,x}\,\mathrm{d}x + \int_a^L b e_{313} u_{3,x}\,\mathrm{d}x = b e_{313}[u_3(L) - u_3(0)] \tag{7}$$

Equation (7) shows that the total charge output, which includes the charges generated by the perfectly bonded and debonded parts, measures the average stain of the entire beam.

When the charge is differentiated with respect to time, the current output of the sensor can be obtained as

$$I(t) = \int_0^a b e_{313} u_{3,xt}\,\mathrm{d}x + \int_a^L b e_{313} u_{3,xt}\,\mathrm{d}x$$
$$= b e_{313}[u_{3,t}(L) - u_{3,t}(0)] \tag{8}$$

To perform the vibration control of the smart beam, the control laws should be designed to determine the control voltage applied on the piezoelectric actuators. Direct feedback control for the collocated sensor and actuator is widely used. According to the PD control law, the control voltage is simply designed as

$$V(t) = -g_1 q(t) - g_2 I(t) \tag{9}$$

where g_1 and g_2 are control gains.

When the following notations are introduced:

$$\eta_i = \frac{\rho_i L^2}{E_2}, \qquad \alpha_2 = \frac{h_2}{L}, \qquad \beta_i = \frac{E_i}{E_2}$$

$$\varphi_i = \frac{h_i}{h_2}, \qquad \varphi_{vj} = \frac{h_{vj}}{h_2}, \qquad \beta_{vj} = \frac{E_{vj}}{E_2}, \qquad j = 1, 3$$

$$\xi = \frac{x}{L}, \qquad u_{ni} = \frac{u_i}{h_2}, \qquad w_{ni} = \frac{w_i}{h_2}$$

$$T_{ni} = \frac{T_i}{E_2 b h_2}, \qquad Q_{ni} = \frac{Q_i}{E_2 b h_2}, \qquad i = 1, 2, 3$$

$$M_{ni} = \frac{M_i}{E_2 b h_2^2/12}, \qquad t_n = \frac{t}{L^2}\sqrt{\frac{E_2 h_2^2}{12\rho_2}}, \qquad V_n(t_n) = \frac{e_{311} V(t)}{E_2 h 2} \tag{10}$$

Eqs. (1–5) can be nondimensionalized as

$$m_1 k_t^2 \ddot{u}_{n1} = T_{n1,\xi} + \tau_{n1}, \qquad m_1 k_t^2 \ddot{w}_{n1} = Q_{n1,\xi} + \sigma_{n1}$$

$$M_{n1,\xi} + 6\varphi_1 \tau_{n1} - (12/\alpha_2) Q_{n1} = 0$$

$$m_2 k_t^2 \ddot{u}_{n2} = T_{n2,\xi} - \tau_{n1} + \tau_{n3} + f_{nl}(\xi, t_n)$$

$$m_2 k_t^2 \ddot{w}_{n2} = Q_{n2,\xi} - \sigma_{n1} + \sigma_{n3} + f_{nt}(\xi, t_n)$$

$$M_{n2,\xi} + 6\varphi_2(\tau_{n1} + \tau_{n3}) - (12/\alpha_2) Q_{n2} = 0 \tag{11}$$

$$m_3 k_t^2 \ddot{u}_{n3} = T_{n3,\xi} - \tau_{n3}, \qquad m_3 k_t^2 \ddot{w}_{n3} = Q_{n3,\xi} - \sigma_{n3}$$

$$M_{n3,\xi} + 6\varphi_3 \tau_{n3} - (12/\alpha_2) Q_{n3} = 0, \qquad T_{n1} = \beta_1 \alpha_1 u_{n1,\xi} - V_n$$

$$M_{n1} = -\beta_1 \varphi_1 \alpha_1^2 w_{n1,\xi\xi}, \qquad T_{n2} = \beta_2 \alpha_2 u_{n2,\xi}$$

$$M_{n2} = -\beta_2 \varphi_2 \alpha_2^2 w_{n2,\xi\xi}, \qquad T_{n3} = \beta_3 \alpha_3 u_{n3,\xi}$$

$$M_{n3} = -\beta_3 \varphi_3 \alpha_3^2 w_{n3,\xi\xi}$$

$$\tau_{n1} = k_1 r_{a1}\left[u_{n2} - u_{n1} + \tfrac{1}{2}(\alpha_1 w_{n1,\xi} + \alpha_2 w_{n2,\xi})\right]$$

$$\tau_{n3} = k_3 r_{a3}\left[u_{n3} - u_{n2} + \tfrac{1}{2}(\alpha_2 w_{n2,\xi} + \alpha_3 w_{n3,\xi})\right]$$

$$\sigma_{n1} = k_1 r_{a1}^e (w_{n2} - w_{n1}), \qquad \sigma_{n3} = k_3 r_{a3}^e (w_{n3} - w_{n2})$$

where the double dot represents the second derivation with respect to nondimentional time t_n and the parameters are defined as

$$\alpha_i = \varphi_i \alpha_2, \qquad m_i = \alpha_i \eta_i, \qquad \alpha_v = \varphi_v \alpha_2, \qquad i = 1, 2, 3$$

$$k_v = \frac{1 - \nu}{(1 - 2\nu)(1 + \nu)}, \qquad k_g = \frac{1}{2(1 + \upsilon)},$$

$$r_{aj} = \frac{k_g \beta_{vj}}{\alpha_{vj}}, \qquad r_{aj}^e = \frac{k_v \beta_{vj}}{\alpha_{vj}}, \qquad j = 1, 3$$

$$f_{nl} = \frac{L f_l}{E_2 b h_2}, \qquad f_{nt} = \frac{L f_t}{E_2 b h_2}, \qquad k_t = \frac{1}{L^2}\sqrt{\frac{E_2 h_2^2}{12\rho_2}} = \sqrt{\frac{\alpha_2^3}{12 m_2}} \tag{12}$$

When Eqs. (7) and (8) are substituted into Eq. (9), the nondimensionalized control voltage becomes

$$V_n(t_n) = -g_{n1}[u_{3n}(1) - u_{3n}(0)] - g_{n2}[\dot{u}_{3n}(1) - \dot{u}_{3n}(0)] \tag{13}$$

where g_{n1} and g_{n2} are the nondimensional control gains given by

$$g_{n1} = g_1 b e_{311} e_{313}/E_2, \qquad g_{n2} = g_2 b e_{311} e_{313} k_t/E_2 \tag{14}$$

When the state vector is introduced,

$$\boldsymbol{Y}(x) = (u_{n1}, T_{n1}, w_{n1}, w_{n1,x}, Q_{n1}, M_{n1}, u_{n2}, T_{n2}, w_{n2},$$
$$w_{n2,x}, Q_{n2}, M_{n2}, u_{n3}, T_{n3}, w_{n3}, w_{n3,x}, Q_{n3}, M_{n3})^T$$

and only the applied voltage is considered, that is, $f_{nl} = f_{nt} = 0$, Eq. (11) can be rearranged in the following state form:

$$\boldsymbol{Y}_{,\xi} = \boldsymbol{M}\ddot{\boldsymbol{Y}} + \tilde{\boldsymbol{A}}\boldsymbol{Y} + \boldsymbol{B}V_n, \qquad 0 < \xi < 1 \tag{15}$$

where $\boldsymbol{M} \in R^{18\times 18}$ is the mass matrix, $\tilde{\boldsymbol{A}} \in R^{18\times 18}$ is the state matrix, and $\boldsymbol{B} \in R^{18}$ is the vector related to the control voltage on the actuator layer.

For the closed-loop system, when Eq. (13) is noted, the control voltage V_n can be expressed as

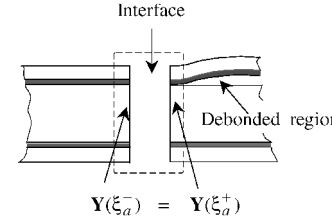

Fig. 2 Continuity conditions at the interface between the perfectly bonded and debonded regions.

$$\boldsymbol{B}V_n(t_n) = \tilde{\boldsymbol{G}}_1[\boldsymbol{Y}(1) - \boldsymbol{Y}(0)] + \tilde{\boldsymbol{G}}_2[\dot{\boldsymbol{Y}}(1) - \dot{\boldsymbol{Y}}(0)] \tag{16}$$

where $\tilde{\boldsymbol{G}}_1$ and $\tilde{\boldsymbol{G}}_2$ are 18×18 matrices. When Eq. (16) is substituted into Eq. (15), the following equations of the closed loop system can be obtained:

$$\boldsymbol{Y}_{,\xi} = \boldsymbol{M}\ddot{\boldsymbol{Y}} + \tilde{\boldsymbol{A}}\boldsymbol{Y} + \tilde{\boldsymbol{G}}_1[\boldsymbol{Y}(1) - \boldsymbol{Y}(0)]$$
$$+ \tilde{\boldsymbol{G}}_2[\dot{\boldsymbol{Y}}(1) - \dot{\boldsymbol{Y}}(0)], \qquad 0 < \xi < 1 \tag{17}$$

Equation (17) is the state form of the equations of motion of the actively controlled beam with piezoelectric actuator/sensor layer including debonding. The continuity and boundary conditions of the beam are given next.

At the interface between the perfectly bonded and debonded regions, the continuity conditions of all displacements and the equilibrium conditions of the stress resultants should be imposed, as shown in Fig. 2. All of these continuity conditions can be expressed as

$$\boldsymbol{Y}\left(\xi_a^-\right) = \boldsymbol{Y}\left(\xi_a^+\right) \tag{18}$$

In general, the boundary conditions of the beam can be expressed as

$$\boldsymbol{D}_0\boldsymbol{Y}(0) + \boldsymbol{D}_L\boldsymbol{Y}(1) = \boldsymbol{D} \qquad \text{for} \qquad \forall t_n \tag{19}$$

where $\boldsymbol{D}_0 \in R^{18\times 18}$, $\boldsymbol{D}_L \in R^{18\times 18}$, and $\boldsymbol{D} \in R^{18}$ are known matrices and vectors corresponding to the given boundary conditions. When the boundary conditions are homogeneous, $\boldsymbol{D} = 0$.

IV. Control Stability Analysis

To analyze the stability of vibration control of the beam with a partly debonded actuator/sensor, assume that the state vector can be separated as

$$\boldsymbol{Y}(\xi, t_n) = \bar{\boldsymbol{Y}}(\xi)\exp(\lambda t_n) \tag{20}$$

where $\bar{\boldsymbol{Y}}(\xi)$ is a function of spatial variable ξ and λ is a characteristic parameter (eigenvalue). Substituting Eq. (20) into Eq. (17) gives

$$\bar{\boldsymbol{Y}}_{,\xi} = \boldsymbol{A}(\lambda)\bar{\boldsymbol{Y}} + \boldsymbol{G}(\lambda)[\bar{\boldsymbol{Y}}(1) - \bar{\boldsymbol{Y}}(0)], \qquad 0 < \xi < 1 \tag{21}$$

where $\boldsymbol{A}(\lambda) = \tilde{\boldsymbol{A}} + \lambda^2\boldsymbol{M}$ and $\boldsymbol{G}(\lambda) = \tilde{\boldsymbol{G}}_1 + \lambda\tilde{\boldsymbol{G}}_2$. Equation (21) becomes an ordinary differential equation with parameter λ, which is very complicated, particularly for the debonding case. For the beam with perfectly bonded actuator ($k_1 = 1$) and debonded actuator ($k_1 = 0$), respectively, state equation (21) has a different form, that is,

$$\bar{\boldsymbol{Y}}_{,\xi} = \boldsymbol{A}_1(\lambda)\bar{\boldsymbol{Y}} + \boldsymbol{G}(\lambda)[\bar{\boldsymbol{Y}}(1) - \bar{\boldsymbol{Y}}(0)], \qquad 0 < \xi \le \xi_a = a/L$$
$$\bar{\boldsymbol{Y}}_{,\xi} = \boldsymbol{A}_2(\lambda)\bar{\boldsymbol{Y}} + \boldsymbol{G}(\lambda)[\bar{\boldsymbol{Y}}(1) - \bar{Y}(0)], \qquad \xi_a < \xi < 1 \tag{22}$$

The solutions of Eq. (22) can be expressed as

$$\bar{\boldsymbol{Y}}(\xi) = \boldsymbol{\Phi}_1(\lambda, \xi)\bar{\boldsymbol{Y}}(0) + \boldsymbol{\Psi}_1(\lambda, \xi)[\bar{\boldsymbol{Y}}(1) - \bar{\boldsymbol{Y}}(0)], \qquad 0 < \xi \le \xi_a$$
$$\bar{\boldsymbol{Y}}(\xi) = \boldsymbol{\Phi}_2(\lambda, \xi - \xi_a)\bar{\boldsymbol{Y}}(\xi_a) + \boldsymbol{\Psi}_2(\lambda, \xi)[\bar{\boldsymbol{Y}}(1) - \bar{\boldsymbol{Y}}(0)]$$
$$\xi_a < \xi \le 1 \tag{23}$$

where the transition matrix $\boldsymbol{\Phi}_i(\lambda, \xi)$ and the matrices $\boldsymbol{\Psi}_1 \in R^{18\times 18}$ and $\boldsymbol{\Psi}_2 \in R^{18\times 18}$ are given by

$$\Phi_i(\lambda, \xi) = e^{A_i(\lambda)\xi}$$

$$\Psi_1(\lambda, \xi) = \left[\int_0^{\xi} \Phi_1(\lambda, \xi - x)\, dx\right] G(\lambda)$$

$$\Psi_2(\lambda, \xi) = \left[\int_{\xi_a}^{\xi} \Phi_2(\lambda, \xi - x)\, dx\right] G(\lambda) \tag{24}$$

From Eq. (23), we have

$$\bar{Y}(\xi_a) = \Phi_1(\lambda, \xi_a)\bar{Y}(0) + \Psi_1(\lambda, \xi_a)[\bar{Y}(1) - \bar{Y}(0)] \tag{25}$$

Substituting Eq. (25) into the second equation in Eq. (23) yields

$$\bar{Y}(\xi) = \Phi_1(\lambda, \xi)\bar{Y}(0) + \Psi_1(\lambda, \xi)[\bar{Y}(1) - \bar{Y}(0)], \qquad 0 < \xi \le \xi_a$$

$$\bar{Y}(\xi) = \Phi_d(\lambda, \xi)\bar{Y}(0) + \boldsymbol{H}_d(\lambda, \xi)[\bar{Y}(1) - \bar{Y}(0)], \qquad \xi_a < \xi \le 1 \tag{26}$$

where

$$\Phi_d(\lambda, \xi) = \Phi_2(\lambda, \xi - \xi_a)\Phi_1(\lambda, \xi_a)$$

$$\boldsymbol{H}_d(\lambda, \xi) = [\Phi_2(\lambda, \xi - \xi_a)\Psi_1(\lambda, \xi_a) + \Psi_2(\lambda, \xi)] \quad (\xi > \xi_a) \tag{27}$$

Equation (26) gives the solution to state equation (21) in terms of $\bar{Y}(0)$, which can be obtained by the following procedure. The state at the right end of the beam can be expressed from Eq. (26) as

$$\bar{Y}(1) = \Phi_d(\lambda, 1)\bar{Y}(0) + \boldsymbol{H}_d(\lambda, 1)[\bar{Y}(1) - \bar{Y}(0)] \tag{28}$$

When the boundary conditions of the beam in Eq. (19) are noted together with Eq. (28), the state vector at the two ends of the beam can be solved by

$$\begin{bmatrix} \Phi_d(\lambda, 1) - \boldsymbol{H}_d(\lambda, 1) & \boldsymbol{H}_d(\lambda, 1) - \boldsymbol{I} \\ \boldsymbol{D}_0 & \boldsymbol{D}_L \end{bmatrix} \begin{Bmatrix} \bar{Y}(0) \\ \bar{Y}(1) \end{Bmatrix} = \begin{Bmatrix} \boldsymbol{0} \\ \bar{\boldsymbol{D}} \end{Bmatrix} \tag{29}$$

For the homogeneous boundary conditions, the nontrivial solution can be obtained only when

$$\det\begin{bmatrix} \Phi_d(\lambda, 1) - \boldsymbol{H}_d(\lambda, 1) & \boldsymbol{H}_d(\lambda, 1) - \boldsymbol{I} \\ \boldsymbol{D}_0 & \boldsymbol{D}_L \end{bmatrix} = 0 \tag{30}$$

Equation (30) is a transcendental equation known as a characteristic equation for the closed-loop control system, which can give complex eigenvalues of the controlled beam. If all of the eigenvalues have nonpositive real parts, the control of the beam is stable.

In general, the elements in the characteristic determinant in Eq. (30) may extremely large because the thin adhesive layer makes the transition matrix over a long span ill conditioned. For example, the elements of the transition matrix from the left end ($\xi = 0$) to the right ($\xi = 1$) may reach the order of 10^{150}. Therefore, although compact characteristic equation (30) looks concise, it may not be used directly to find the eigenvalues with satisfactory accuracy. To solve this problem, we have to bridge the two ends of the beam with some relay points so that the elements of the transition matrix between the adjacent relay points are normal, as shown in Fig. 3. We have to trade between the order of the characteristic determinant and the order of its elements. To this end, set m relay points between $\xi = 0$ and $\xi = \xi_a$ in the part with the perfectly bonded actuator/sensor layer and n points between $\xi = \xi_a$ and $\xi = 1$ in the part with the debonded actuator/sensor layer. When the relay points are denoted ξ_{11}, $\xi_{12}, \ldots, \xi_{1m}$ and $\xi_{21}, \xi_{22}, \ldots, \xi_{2n}$, respectively, Eq. (26) can be changed to the following form:

$$\bar{Y}(\xi_{11}) = \Phi_{11}(\lambda)\bar{Y}(0) + \Psi_{11}(\lambda)[\bar{Y}(1) - \bar{Y}(0)]$$

$$\bar{Y}(\xi_{12}) = \Phi_{12}(\lambda)\bar{Y}(\xi_{11}) + \Psi_{12}(\lambda)[\bar{Y}(1) - \bar{Y}(0)]$$

$$\vdots$$

$$\bar{Y}(\xi_{1m}) = \Phi_{1m}(\lambda)\bar{Y}(\xi_{1m-1}) + \Psi_{1m}(\lambda)[\bar{Y}(1) - \bar{Y}(0)]$$

$$\bar{Y}(\xi_a) = \Phi_{1a}(\lambda)\bar{Y}(\xi_{1m}) + \Psi_{1a}(\lambda)[\bar{Y}(1) - \bar{Y}(0)]$$

$$\bar{Y}(\xi_{21}) = \Phi_{21}(\lambda)\bar{Y}(\xi_a) + \Psi_{21}(\lambda)[\bar{Y}(1) - \bar{Y}(0)]$$

$$\vdots$$

$$\bar{Y}(\xi_{2n}) = \Phi_{2n}(\lambda)\bar{Y}(\xi_{2n-1}) + \Psi_{2n}(\lambda)[\bar{Y}(1) - \bar{Y}(0)]$$

$$\bar{Y}(1) = \Phi_{2e}(\lambda)\bar{Y}(\xi_{2n}) + \Psi_{2e}(\lambda)[\bar{Y}(1) - \bar{Y}(0)] \tag{31}$$

where $\Phi_{1j}(\lambda)$, $\Psi_{1j}(\lambda)$, $j = 1, 2, \ldots, m$, and $\Phi_{2j}(\lambda)$, $\Psi_{2j}(\lambda)$, $j = 1, 2, \ldots, n$ can be obtained from Eq. (24) by replacing ξ with the distance between the adjacent points. Equation (31) together with the homogeneous boundary conditions can be writen as follows:

$$\boldsymbol{R}(\lambda)\boldsymbol{Z} = 0 \tag{32}$$

where $\boldsymbol{Z} = [\bar{Y}^T(0), \bar{Y}^T(\xi_{11}), \ldots, \bar{Y}^T(\xi_{1m}), \bar{Y}^T(\xi_a), \bar{Y}^T(\xi_{21}), \ldots, \bar{Y}^T(\xi_{2n}), \bar{Y}^T(1)]^T$ is the vector consisting of all of the state vectors in the relay points, two ends, and the interface point and

$$\boldsymbol{R}(\lambda) = \begin{bmatrix}
\Phi_{11} - \Psi_{11} & -\boldsymbol{I} & & & & & & \Psi_{11} \\
-\Psi_{12} & \Phi_{12} & -\boldsymbol{I} & & & & & \Psi_{12} \\
\vdots & \vdots & \ddots & & & & & \vdots \\
-\Psi_{1m} & \boldsymbol{0} & & \Phi_{1m} & -\boldsymbol{I} & & & \Psi_{1m} \\
-\Psi_{1a} & \boldsymbol{0} & & & \Phi_{1a} & -\boldsymbol{I} & & \Psi_{1a} \\
-\Psi_{21} & \boldsymbol{0} & & & & \Phi_{21} & -\boldsymbol{I} & \Psi_{21} \\
\vdots & \vdots & & & & & \ddots & \vdots \\
-\Psi_{2e} & \boldsymbol{0} & & & & & \Phi_{2e} & \Psi_{2e} - \boldsymbol{I} \\
\boldsymbol{D}_0 & \boldsymbol{0} & & & & & & \boldsymbol{D}_L
\end{bmatrix} \tag{33}$$

Once again, to obtain the nontrivial solution of $\boldsymbol{Z}$, the following condition must be satisfied:

$$\det[\boldsymbol{R}(\lambda)] = 0 \tag{34}$$

It is clear that Eq. (34) is the characteristic equation of the controlled beam with a debonded piezoelectric actuator/sensor layer. Note that the eigenvalues obtained from Eq. (34) do not depend on the number of the relay points m and n. In fact, when properties of the transition matrices are employed and the state vectors at the relay points in Eq. (31) are eliminated, one can obtain the same equations in Eq. (29). Furthermore, by the introduction of the relay points in the span of the beam, multiple debonding regions in the beam can be readily dealt with.

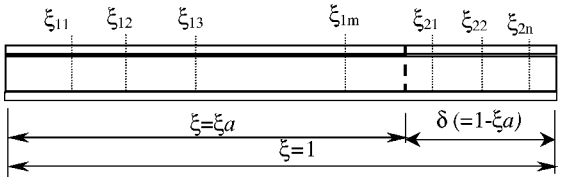

Fig. 3 Relay points in the entire beam.

V. Determination of Critical Debonding Length

The critical debonding length for a given controlled mode can be defined as the maximum debonding length it can sustain before loss of control. To investigate the tolerance of a given mode of the beam to actuator debonding, its critical debonding length should be determined.

Denote the ith eigenvalue as

$$\lambda_i = n_i + \Omega_{di} I \tag{35}$$

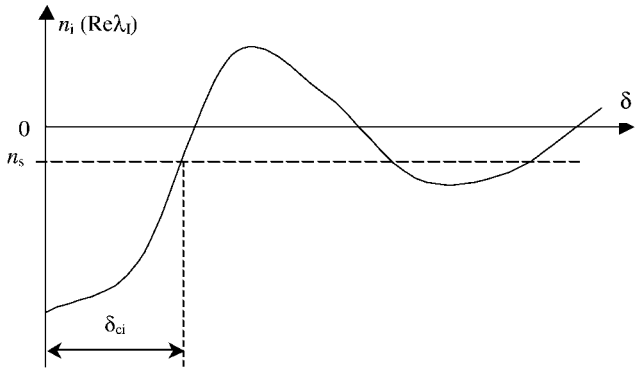

Fig. 4 Determination of critical debonding length at given damping threshold.

where $I = \sqrt{-1}$ is the imaginary unit, n_i is the active damping coefficient, and Ω_{di} is the frequency of the actively damped beam. Theoretically, when Eq. (20) is noted, the control stability of this mode can be examined according to the following criteria.

Asymptotically stable:

$$n_i < 0 \tag{36a}$$

Stable (oscillation):

$$n_i = 0 \tag{36b}$$

Unstable:

$$n_i > 0 \tag{36c}$$

The real part n_i for each mode is also an indicator of its stability degree. A smaller n_i indicates the mode is more stable. Therefore, from a practical viewpoint, it is usually expected that the controlled mode is more stable, which means that it can decay faster than a designated rate. In other words, only when the active damping coefficient is less than a given damping threshold $n_s \leq 0$, the corresponding control of the mode is deemed acceptable, that is,

Control is acceptable:

$$n_i \leq n_s \tag{37a}$$

Control is not acceptable:

$$n_i > n_s \tag{37b}$$

In this case, the satisfactorily controlled mode should exponentially decay with a rate not less than $e^{-|n_s|t_n}$.

When a debonding of the actuator occurs, both real and imaginary parts of the eigenvalues of the beam will vary with the debonding length. A typical curve of the real part of an eigenvalue vs debonding length of the actuator is schematically given in Fig. 4. Because the original closed-loop control is assumed to be stable, the real part n_i of each controlled mode approaches zero from an initial negative value as the debonding length increases. For a given threshold n_s, the critical debonding length δ_{ci} for this mode can be found at which its real part crosses the line $n_i = n_s$ the first time, as shown in Fig. 4. The critical debonding length that the whole system can tolerate will be the smallest one in the critical debonding lengths of all controlled modes. Note that the stability of the additional modes induced by the debonding is another key factor affecting the critical debonding length of the beam when a debonding of the piezoelectric layer occurs.

In practice, the natural damping is inevitable. In this case, both the inherent damping and the active control will contribute to the damping ratio n_i. Because the natural damping always provides positive damping, the system can still be acceptable even if the active control provides negative damping due to the actuator debonding, as long as Eq. (37a) can still be satisfied. Therefore, the natural damping can enlarge the critical debonding length.

VI. Examples and Analysis

In this section, three examples are presented to examine the effects of edge debondings of the actuator layer on the control stability of the controlled beam using PD control. In the examples, a cantilevered host beam with fully covered piezoelectric actuator and sensor layers in its upper and lower surfaces is considered, as shown in Fig. 1. The parameters are taken as $\nu_1 = \nu_3 = 0.34$, $\alpha_2 = 0.007$, $\beta_1 = \beta_3 = 0.3$, $\beta_{v1} = \beta_{v3} = 0.01$, $\eta_1 = \eta_3 = 3.2 \times 10^{-9}$, $\eta_2 = 3.5 \times 10^{-9}$, $\varphi_1 = \varphi_3 = 0.4$, $\varphi_{v1} = \varphi_{v3} = \frac{1}{14}$, $\beta_2 = \varphi_2 \equiv 1$, $g_{n1} = 0$, and $g_{n2} = 5.12 \times 10^{-5}$. The parameter k_t can be calculated as 34.16, which can be used to convert the nondimensional eigenvalues to corresponding physical ones using Eq. (10).

The method for stability analysis in this paper is developed based on the established model presented in Ref. 14, in which the mathematical model has been validated by comparing the experimental and numerical results given by Seely and Chattopadhyay[8,9] and an equivalent model. The comparison shows that the frequencies obtained by the current model are in good agreement with the experimental and finite element results for both the perfect bonding and the debonding cases. Moreover, it also shows that the first three peak values in the frequency spectrum of a controlled beam obtained from this model is also in good agreement with those from an equivalent model[14] when the adhesive layers are very thin.

A. Edge Debonding in Actuator at Free End

To examine the effects of the edge debonding of the actuator layer at the free end of the beam on the control stability of the cantilevered beam, an edge debonding of the piezoelectric actuator layer is introduced at the free end of the beam. For different debonding length δ, 5, 10, 15, 20, 25, and 30% of the undebonded actuator length, the first nine eigenvalues of the closed-loop system whose frequencies are less than 1000 are calculated from Eq. (33) and are listed in Table 1. In addition, due to vibration of the debonded part of the actuator layer, additional eigenvalues of the debonded portion of the actuator whose frequencies are below 1000 are also determined and given in Table 1. Each eigenvalue corresponds to one vibration mode, whose real and imaginary parts are the damping coefficient and frequency of this actively damped mode, respectively.

Because the real parts of the eigenvalues are used to determine control stability of the their related vibration modes, they are plotted in Fig. 5 vs different debonding lengths of the actuator layer. As shown in Fig. 5 and Table 1, all of the first nine eigenvalues of the controlled beam with perfectly bonded piezoelectric actuator and sensor layers have negative real parts, which indicates that the first nine modes of the closed-loop system are stable. In this case, the eighth eigenvalue has the maximum real part, and this vibration mode decays most slowly, which means this mode can not be effectively controlled. When a 5% edge debonding of the actuator layer occurs at the free end of the beam, the real parts of all of the first nine eigenvalues still remain negative, although their absolute values become smaller. A 10% edge debonding of the actuator will destabilize the control of the eighth and ninth modes of the closed-loop system because the real parts of these two eigenvalues become positive. As the debonding length of the actuator increases further, more lower-order modes of the controlled beam become unstable. For example, control of the sixth mode is no longer stable when a 15% edge debonding occurs, and the lowest unstable modes are mode 5, 4, and 3 for 20, 25, and 30% debonding, respectively.

Figure 5 also shows that a lower mode can sustain a larger debonding, whereas a higher mode can only tolerate a smaller debonding. For a zero damping threshold, $n_s = 0$, the critical debonding length for mode 4 is about 20%, and mode 9 can only sustain a debonding less than 9%. The critical debonding length for the entire system is determined by the minimum one of all of the critical debonding lengths for all controlled modes. For example, when the first nine modes are controlled, the critical debonding length that the whole system can sustain is about 6%, above which the control of mode 8 will become unstable. In this case, the original closed-loop control will collapse if no measure is taken to prevent it from happening or to remedy the system.

To examine the stability of the controlled beam with a partially debonding actuator, in addition to the modes of the composite beam with debonded actuator, the additional modes due to vibration of the debonded portion of the actuator must be considered. In fact, the additional modes may be more critical in judging the stability of the closed-loop system because the original control system was designed to control the original system and may act as an excitation

Table 1 Eigenvalues of the controlled beam with actuator and sensor pair and additional eigenvalues caused by the edge debonding of the actuator at the free end

Mode no.	Debonding length, %						
	0	5	10	15	20	25	30
1	$-0.0949 \pm 4.181I$	$-0.0948 \pm 4.180I$	$-0.0947 \pm 4.180I$	$-0.0942 \pm 4.178I$	$-0.0930 \pm 4.171I$	$-0.0904 \pm 4.153I$	$-0.0850 \pm 4.111I$
2	$-1.1305 \pm 26.074I$	$-1.1234 \pm 26.057I$	$-1.0914 \pm 25.981I$	$-0.9004 \pm 25.403I$	$-1.0491 \pm 27.692I$	$-1.0011 \pm 26.848I$	$-0.8407 \pm 26.422I$
3	$-2.7723 \pm 72.310I$	$-2.6664 \pm 72.192I$	$-1.4724 \pm 69.202I$	$-2.2995 \pm 73.554I$	$-1.5723 \pm 72.437I$	$-0.4716 \pm 69.860I$	$0.2545 \pm 71.787I$
4	$-3.9958 \pm 140.305I$	$-3.5501 \pm 139.942I$	$-3.2066 \pm 142.601I$	$-1.7776 \pm 140.757I$	$-0.0906 \pm 142.629I$	$1.6190 \pm 139.921I$	$2.3336 \pm 138.537I$
5	$-3.5872 \pm 231.126I$	$-2.6635 \pm 229.110I$	$-2.0700 \pm 233.330I$	$0.2370 \pm 211.949I$	$1.6768 \pm 232.121I$	$2.4528 \pm 238.401I$	$3.1067 \pm 233.925I$
6	$-2.1103 \pm 345.878I$	$-1.7029 \pm 355.853I$	$-0.6717 \pm 346.342I$	$0.7253 \pm 346.801I$	$0.9395 \pm 359.112I$	$1.7097 \pm 347.969I$	$-0.0896 \pm 342.051I$
7	$-0.6853 \pm 484.457I$	$-0.5460 \pm 489.491I$	$0.1040 \pm 462.531I$	$0.4673 \pm 480.914I$	$0.5854 \pm 484.421I$	$0.0202 \pm 478.979I$	$-0.0502 \pm 507.224I$
8	$-0.0033 \pm 646.352I$	$-0.0012 \pm 649.517I$	$0.0066 \pm 641.617I$	$0.0116 \pm 646.695I$	$0.0095 \pm 632.204I$	$-0.0135 \pm 627.578I$	$-0.0083 \pm 632.744I$
9	$-0.8919 \pm 831.430I$	$-0.6990 \pm 831.436I$	$0.2483 \pm 814.510I$	$0.3075 \pm 815.771I$	$-0.1188 \pm 811.824I$	$-0.4594 \pm 816.781I$	$-0.0640 \pm 807.975I$
A1	——	$0.0008 \pm 302.697I$	$-0.9948 \pm 84.364I$	$-0.1853 \pm 37.429I$	$-0.0401 \pm 19.816I$	$-0.0018 \pm 13.281I$	$-0.0131 \pm 9.480I$
A2	——	——	$-0.0597 \pm 498.968I$	$-0.2466 \pm 237.258I$	$0.1666 \pm 120.913I$	$-0.1281 \pm 80.969I$	$0.0593 \pm 54.471I$
A3	——	——	——	$0.0027 \pm 606.912I$	$0.6150 \pm 337.837I$	$0.3536 \pm 219.798I$	$0.3986 \pm 157.939I$
A4	——	——	——	——	$-0.0001 \pm 675.848I$	$-0.0890 \pm 430.594I$	$-0.1778 \pm 300.250I$
A5	——	——	——	——	——	$0.0007 \pm 721.853I$	$-0.0502 \pm 507.224I$
A6	——	——	——	——	——	——	$0.0014 \pm 744.848I$

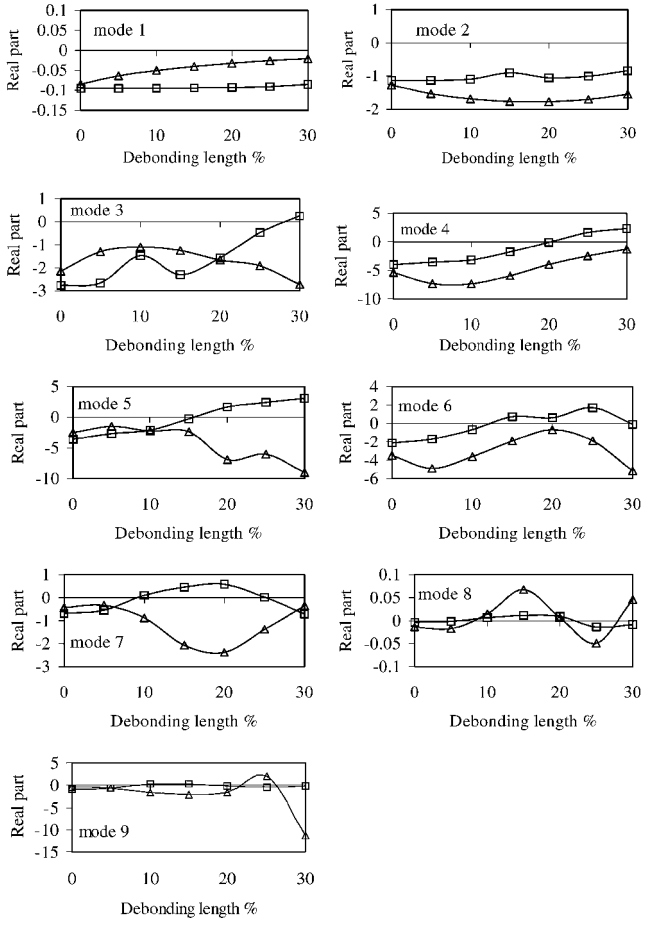

Fig. 5 Real parts of the eigenvalues of the controlled beam with different debonding lengths of the actuator layer: □, debonding at free end and △, debonding at the root end.

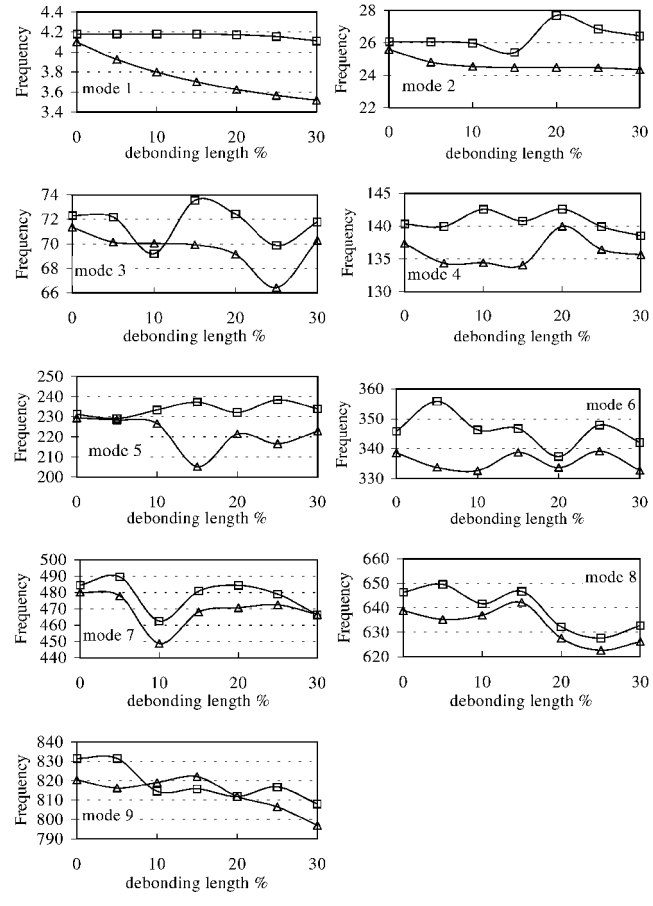

Fig. 6 Nondimensional frequencies of the controlled beam with different debonding lengths of the actuator layer: □, debonding at free end and △, debonding at the root end.

to the debonded part of the actuator when a debonding of the actuator occurs. In return, when the vibration of the debonded portion of the actuator becomes unstable, it then has an adverse effect on the vibration control of the whole beam system. It can be seen from Table 1 that there exists at least one unstable additional mode with different debonding length. Even for a 5% edge debonding of the actuator layer, the first additional mode appears as an unstable mode, the eigenvalue of which has a positive real part.

When the additional modes due to vibration of the debonded portion of the actuator are considered, the critical debonding length the whole system can tolerate may further decrease. For example, the first nine modes can sustain up to a 6% edge debonding of the actuator layer, but the additional mode cannot tolerate a 5% debonding. Moreover, when a modal frequency of the composite beam is close to an additional modal frequency, its damping coefficient (real part of the related eigenvalue) is altered significantly. Therefore, the stability of the debonded part of the actuator may play a special role in determining the control stability of the whole system.

The relationship of the frequencies of the actively damped beam and the debonding length of the actuator layer is presented in Fig. 6. Figure 6 shows that the edge debonding of the actuator at the free end of the clamped beam has a remarkable effect on the frequencies of the controlled beam. Moreover, the vibration mode of the debonded portion of the actuator layer has a special effect on the frequencies of the modes whose frequencies are close to it. In general, the frequency of each additional mode lies between two consecutive modal

Table 2 Eigenvalues of the controlled beam with self-sensing actuator and additional eigenvalues caused by edge debonding of the actuator at the free end

Mode no.	Debonding length,%						
	0	5	10	15	20	25	30
1	$-0.0958 \pm 3.869I$	$-0.0957 \pm 3.868I$	$-0.0954 \pm 3.8687I$	$-0.0944 \pm 3.867I$	$-0.0925 \pm 3.861I$	$-0.0887 \pm 3.845I$	$-0.0820 \pm 3.805I$
2	$-1.1042 \pm 24.47I$	$-1.0749 \pm 24.507I$	$-1.0046 \pm 24.469I$	$-0.7902 \pm 23.923I$	$-0.714654 \pm 27.003I$	$-0.6255 \pm 25.618I$	$-0.4081 \pm 24.931I$
3	$-2.2468 \pm 69.145I$	$-1.9385 \pm 69.131I$	$-1.0405 \pm 66.095I$	$-0.9576 \pm 70.517I$	$-0.3639 \pm 68.124I$	$-0.0295 \pm 64.684I$	$-0.0074 \pm 66.942I$
4	$-2.5036 \pm 135.531I$	$-1.8285 \pm 134.710I$	$-1.0609 \pm 137.366I$	$-0.2447 \pm 132.145I$	$-0.0028 \pm 135.082I$	$-0.1346 \pm 128.463I$	$-0.2664 \pm 127.568I$
5	$-2.0224 \pm 222.669I$	$-1.1961 \pm 218.949I$	-0.4364 ± 220.876	$-0.0106 \pm 203.141I$	$-0.1509 \pm 213.107I$	$-0.1953 \pm 210.236I$	$-0.1316 \pm 213.811I$
6	$-1.3487 \pm 330.162I$	$-0.5619 \pm 345.910I$	$-0.0779 \pm 323.137I$	$-0.0688 \pm 320.367I$	$-0.1857 \pm 316.876I$	$-0.0885 \pm 319.338I$	$-0.0000 \pm 320.884I$
7	$-0.6854 \pm 457.711I$	$-0.3558 \pm 462.792I$	$-0.0040 \pm 436.666I$	$-0.1272 \pm 445.312I$	$-0.0976 \pm 447.955I$	$-0.0006 \pm 451.931I$	$-0.0722 \pm 438.001I$
8	$-0.1518 \pm 604.793I$	$-0.0698 \pm 607.967I$	$-0.0062 \pm 599.118I$	$-0.0102 \pm 624.177I$	$-0.0043 \pm 587.685I$	$-0.0363 \pm 585.357I$	$-0.0414 \pm 589.820I$
9	$-0.0783 \pm 770.152I$	$-0.0415 \pm 773.017I$	$-0.0088 \pm 761.540I$	$-0.0234 \pm 763.047I$	$-0.0003 \pm 758.322I$	$-0.0127 \pm 761.291I$	$-0.0016 \pm 762.762I$
A1	——	$-0.0731 \pm 298.523I$	$-0.3139 \pm 85.3425I$	$-0.0954 \pm 37.972I$	$-0.0863 \pm 19.5707I$	$-0.0001 \pm 13.411I$	$-0.0098 \pm 9.639I$
A2	——	——	$-0.0200 \pm 487.300I$	$-0.0156 \pm 227.963I$	$-0.0155 \pm 117.355I$	$-0.0284 \pm 80.590I$	$-0.0151 \pm 53.498I$
A3	——	——	——	$-0.0520 \pm 586.544I$	$-0.0135 \pm 352.486I$	$-0.0490 \pm 228.726I$	$-0.0051 \pm 157.533I$
A4	——	——	——	——	$-0.0023 \pm 670.98I$	$-0.0046 \pm 421.929I$	$-0.0054 \pm 295.429I$
A5	——	——	——	——	——	$-0.0003 \pm 718.482I$	$-0.0002 \pm 505.412I$
A6	——	——	——	——	——	——	$-0.0002 \pm 732.170I$

Table 3 Eigenvalues of the controlled beam with actuator/sensor layers and additional eigenvalues caused by edge debonding of the actuator at the clamped end

Mode no.	Debonding length, %						
	0	5	10	15	20	25	30
1	$-0.0844 \pm 4.099I$	$-0.0639 \pm 3.923I$	$-0.0504 \pm 3.798I$	$-0.0402 \pm 3.701I$	$-0.0323 \pm 3.624I$	$-0.0260 \pm 3.564I$	$-0.0209 \pm 3.518I$
2	$-1.2689 \pm 25.591I$	$-1.5346 \pm 24.806I$	$-1.6878 \pm 24.531I$	$-1.7684 \pm 24.467I$	$-1.7746 \pm 24.479I$	$-1.7025 \pm 24.463I$	$-1.5497 \pm 24.343I$
3	$-2.1465 \pm 71.356I$	$-1.3015 \pm 70.154I$	$-1.0961 \pm 70.049I$	$-1.2477 \pm 69.922I$	$-1.6598 \pm 69.150I$	$-1.9154 \pm 66.425I$	$-2.7351 \pm 70.284I$
4	$-5.3924 \pm 137.330I$	$-7.3418 \pm 134.331I$	$-7.3900 \pm 134.431I$	$-5.9456 \pm 134.074I$	$-3.9672 \pm 139.976I$	$-2.4994 \pm 136.438I$	$-1.3170 \pm 135.609I$
5	$-2.4939 \pm 229.384I$	$-1.4895 \pm 228.405I$	$-2.2361 \pm 226.608I$	$-2.2452 \pm 205.270I$	$-6.8872 \pm 221.448I$	$-6.0173 \pm 216.510I$	$-9.0044 \pm 222.926I$
6	$-3.4715 \pm 338.639I$	$-4.8924 \pm 333.768I$	$-3.5910 \pm 332.685I$	$-1.9160 \pm 338.803I$	$-0.6843 \pm 333.705I$	$-1.8979 \pm 339.195I$	$-5.1529 \pm 332.732I$
7	$-0.4282 \pm 480.073I$	$-0.3338 \pm 477.842I$	$-0.8758 \pm 448.679I$	$-2.0664 \pm 468.014I$	$-2.3766 \pm 470.616I$	$-1.3787 \pm 472.414I$	$-0.3514 \pm 466.457I$
8	$-0.0134 \pm 638.805I$	$-0.0174 \pm 635.204I$	$0.0147 \pm 636.930I$	$0.0677 \pm 642.098I$	$0.0066 \pm 627.479I$	$-0.0492 \pm 622.604I$	$0.0458 \pm 626.180I$
9	$-0.4246 \pm 820.432I$	$-0.6032 \pm 816.202I$	$-1.7240 \pm 819.067I$	$-2.2557 \pm 822.074I$	$-1.7714 \pm 811.841I$	$2.1029 \pm 806.537I$	$-11.3471 \pm 796.885I$
A1	——	$0.0122 \pm 287.927I$	$-0.0016 \pm 75.923I$	$0.0007 \pm 34.358I$	$-0.0003 \pm 19.502I$	$0.0000 \pm 12.550I$	$0.0000 \pm 8.748I$
A2	——	——	$-0.2559 \pm 499.750I$	$-2.3482 \pm 234.551I$	$-0.5519 \pm 118.361I$	$-0.4522 \pm 81.296I$	$-0.4159 \pm 53.549I$
A3	——	——	——	$-0.0033 \pm 606.689I$	$-0.3452 \pm 355.552I$	$-3.1997 \pm 229.279I$	$-0.2223 \pm 157.687I$
A4	——	——	——	——	$0.0066 \pm 676.002I$	$-0.0744 \pm 430.335I$	$-0.7948 \pm 299.538I$
A5	——	——	——	——	——	$-0.1118 \pm 722.226I$	$-0.0693 \pm 506.666I$
A6	——	——	——	——	——	——	$0.1264 \pm 744.041I$

frequencies of the composite beam, and in most cases, it makes the lower one even lower and the higher one even higher. For example, the first additional mode for a 10% edge debonding (frequency is 84.364) lies between the third and fourth modes of the beam. It suppresses the frequency of the former one from about 72.3 to 69.2 and pushes that of the latter one from 140.3 up to 142.6. This clearly shows that the frequencies of the beam are not simply decreased due to the stiffness reduction of the beam caused by the actuator debonding.

B. Edge Debonding in Self-Sensing Actuator at Free End

As a comparison, the control stability of a cantilevered beam controlled by a self-sensing actuator layer is investigated. The parameters for the host beam and piezoelectric layer used in this case are the same as those in Sec. VI.A. The first nine eigenvalues of the controlled beam with different edge debonding lengths in the actuator are presented in Table 2. In addition, the additional eigenvalues related to the vibration of the debonded part of the actuator are also given in Table 2. As shown in Table 2, not only the first nine modes of the controlled beam but also the additional modes are stable after a debonding of the self-sensing actuator occurs at the free end of the beam. Because the sensor and the actuator are still really collocated after a debonding, the control system can remain stable. The control system using a self-sensing actuator is tolerant to the debonding of the actuator. However, if the threshold n_s is taken as -0.005, the critical debonding length of the entire system will be less than 10% because the control of seventh mode will not be acceptable when a 10% debonding occurs.

C. Edge Debonding in Actuator at Clamped End

Finally, we examine the effect of actuator debonding at the clamped end on the control stability of the beam. In this case, both ends of each piezoelectric layer are free. The eigenvalues of the composite beam for different debonding lengths are calculated and given in Table 3, and the curves of their real and imaginary parts vs debonding length are also shown in Figs. 5 and 6, respectively. It can be clearly seen that the edge debonding of the actuator layer at the root of the beam has much less influence on the control stability of the first nine modes than the debonding at the free end. All of the first nine modes, except mode 8, can tolerate a 25% edge debonding located at the clamped end of the beam. This is probably because the debonded part of the actuator near the root does not vibrate as strongly as it does at the free end, and consequently, it has weaker effects on stability of the controlled modes. However, unstable vibration modes may be induced by vibration of the debonded part of the actuator. For example, even a 5% debonding can induce an unstable mode of the debonded part of the piezoelectric actuator. When the debonding length of the piezoelectric actuator increases, it may lead to more unstable modes in the vibration of the debonded actuator part. Once again, this example also shows that the effects of the debonded part of the actuator may be critical to the control stability of the whole control system when an edge debonding of the actuator occurs.

When Tables 1 and 3 are compared, it can be seen that the debonding near the clamped end of the beam can cause much more significant change in the damping and frequencies than that near the free end. For example, a 30% debonding at the free end results in only a small reduction in damping of the first two modes, whereas a debonding with same length at the clamped end causes a large reduction in damping of the first mode due to the large strain at the clamped end of a cantilever beam. In addition, the debonding at the fixed end leads to an increase in damping of the second, third, fifth, and sixth modes, probably because the shape of the debonded actuator matches these modes more closely.

VII. Conclusions

A scheme for control stability analysis of smart beams with debonded piezoelectric actuator is presented. Based on an 18-dimensional state equation derived from a detailed bending–extension model, a characteristic equation of the beam controlled by partially debonded piezoelectric actuator layer and sensor is derived. The control stability of the controlled mode can be examined by inspecting the real part of its corresponding eigenvalue obtained from the characteristic equation. The critical debonding length for each controlled mode can also be determined from its damping coefficient–debonding length relationship at a given damping threshold. The simulation results show that even a 5% edge debonding of the actuator layer can destabilize the cantilevered beam controlled by a fully covered piezoelectric actuator and sensor that are bonded onto the upper and lower surfaces of the host beam, respectively. It is also found that the beam controlled by a self-sensing actuator layer is tolerant to the edge debonding of the piezoelectric layer.

Acknowledgment

The authors are grateful for the support of the Australia Research Council through Large Grant A10009074.

References

[1]Bailey, T., and Hubbard, J. E., "Distributed Piezoelectric-Polymer Active Vibration Control of a Cantilever Beam," *Journal of Guidance, Control, and Dynamics*, Vol. 8, No. 5, 1985, pp. 605–611.

[2]Im, S., and Atluri, S. N., "Effect of a Piezo-Actuator on a Finitely Deformed Beam Subject to General Loading," *AIAA Journal,* Vol. 27, No. 12, 1989, pp. 1801–1807.

[3]Tzou, H.-S., and Anderson, G. L., *Intelligent Structural Systems*, Kluwer Academic, Dordrecht, The Netherlands, 1992, pp. 9–74.

[4]Crawley, E. F., "Intelligent Structures for Aerospace: A Technology Overview and Assessment," *AIAA Journal*, Vol. 32, No. 8, 1994, pp. 1689–1699.

[5]Chee, C., Tong, L., and Steven, G. P., "A Review on the Modeling of Piezoelectric Sensors and Actuators Incorporated in Intelligent Structures," *Journal of Intelligent Material Systems and Structures*, Vol. 9, No. 1, 1998, pp. 3–19.

[6]Sun, D. C., Wang, D. J., Xu, Z. L., and Li, Y., "Stability and Controllability Analysis of Piezoelectric Smart Plates," *Progress in Natural Science*, Vol. 9, No. 6, 1999, pp. 463–471.

[7]Sun, D. C., and Tong, L., "Modal Control of Smart Shells by Optimized Discretely Distributed Piezoelectric Transducers," *International Journal of Solids and Structures,* Vol. 38, No. 18, 2001, pp. 3281–3299.

[8]Seeley, C. E., and Chattopadhyay, A., "Modeling of Adaptive Composites Including Debonding," *International Journal of Solids and Structures*, Vol. 36, No. 12, 1999, pp. 1823–1843.

[9]Seeley, C. E., and Chattopadhyay, A., "Experimental Investigation of Composite Beams with Piezoelectric Actuation and Debonding," *Smart Materials and Structures*, Vol. 7, No. 4, 1998, pp. 502–511.

[10]Wang, X. D., and Meguid, S. A., "On the Electroelastic Behavior of a Thin Piezoelectric Actuator Attached to an Infinite Host Structures," *International Journal of Solids and Structures*, Vol. 37, No. 23, 2000, pp. 3231–3251.

[11]Tylikowski, A., "Effects of Piezoactuator Delamination on the Transfer Functions of Vibration Control Systems," *International Journal of Solids and Structures*, Vol. 38, No. 10–13, 2001, pp. 2189–2202.

[12]Tong, L., Sun, D. C., and Atluri, S. N., "Sensing and Actuating Behaviors of Piezoelectric Layers with Debonding in Smart Beams," *Smart Materials and Structures*, Vol. 10, No. 4, 2001, pp. 713–723.

[13]Rew, K. H., Han, J. H., and Lee, I., "On-Line Frequency Estimation and Adaptive Vibration Control of Composite Structures with Delaminations," *Key Engineering Materials*, Vol. 183–187, 2000, pp. 1201–1206.

[14]Sun, D., Tong, L., and Atluri, S. N., "Effects of Piezoelectric Sensor/Actuator Debonding on Vibration Control of Smart Beams," *International Journal of Solids and Structures*, Vol. 38, No. 50–51, 2001, pp. 9033–9051.

A. Chattopadhyay
Associate Editor